Eur. Phys. J. B (2018) 91: 245
https://doi.org/10.1140/epjb/e2018-90273-7

THE EUROPEAN PHYSICAL JOURNAL B

Regular Article

Determination of allowed transitions types and the optical parameters of Se–Ge–Ag chalcogenide films

Amira M. Shakra[a] and Essam G. El-Metwally

Semiconductor Laboratory, Physics Department, Faculty of Education, Ain Shams University, Roxy, Cairo, Egypt

Received 22 April 2018 / Received in final form 25 June 2018
Published online 10 October 2018

Abstract. Amorphous $Se_{0.68}Ge_{0.24}Ag_{0.08}$ films were prepared by the known thermal evaporation method. X-ray diffraction (XRD) and energy dispersive X-ray (EDX) analysis were used to identify the structure of the prepared samples. Transmittance $T(\lambda)$ was measured at room temperature in the wave length range (400–2500 nm) for the investigated films of different thicknesses in range (221.2–815.2 nm). Swanepoel's method was used to calculate the index of refraction n and absorption k. The allowed transitions in the studied composition are indirect. Values of optical band gap E_g^{opt} were determined using two different methods. The obtained values of E_g^{opt} are equal 1.90 and 1.91 eV, also the value of Urbach energy E_e equal 0.50 ± 0.01 eV. Dispersion of refractive index n is analyzed using a single-oscillator model. The optical high frequency dielectric constant ε_∞ and the optical dispersion parameters (E_o and E_d) were calculated by analyzing the obtained values of n. The obtained values of E_o, E_d and the average value of ε_∞ are found to be 5.36 eV, 18.86 eV and 4.60, respectively. The ratio N/m^* for the investigated composition is 3.87×10^{55} m^{-3}. The dependence of real ε_1 and imaginary ε_2 parts of dielectric constant, relaxation time τ and the optical conductivity σ_{opt} on photon energy $h\nu$ was also studied for $Se_{0.68}Ge_{0.24}Ag_{0.08}$ films. The obtained results showed that ε_1, ε_2, τ and σ_{opt} increased with photon energy.

1 Introduction

Recently, chalcogenide glasses attracted the attention of scientists in various fields of science and engineering. Solid-state physicists and chemists, in addition to electronic engineers, are interested in their potential applications in different devices. Nowadays, glasses of chalcogenide are widely used in several optoelectronic applications such as infrared optical fibers, microsensing, signal processing, photonic circuits, switching and memory devices, photolithography, in the manufacture of cheap solar cells and as reversible phase change optical recorders [1–6]. The structural and optical properties of different chalcogenide glasses have been studied [7–12] and also, chalcogenides containing Ag had been investigated by several workers [13–19]. Chalcogenide glasses containing Ag have many applications in information storage, optical imaging and photolithography [20]. Also, they are very important materials for guided wave devices in integrated optics because they have good transparency in the infrared region [21]. The addition of Ag to chalcogenides is expected to create both composition and configuration disorder in the material [22]. Silver addition to glassy materials leads to a change in their physical and chemical properties. Addition of Ag to As–Se alloys are used as super ionic conducting glasses. Ag-rich glasses such as Ag–As(Ge)–S exhibit a photo induced segregation of fine Ag particles [23,24]. Ag-based chalcogenides are used in rewritable disks and erasable phase change optical recording devices [25,26], they are preferred because of their ionic nature. Ag^+ ions play an important role in the electrical conduction [27,28].

Many authors studied the effect of Ag as an additive to different chalcogenide glasses. For example a significant decrease of the activation energy and increase in the band tailing is observed as a consequence of silver addition to Ge–Se–Sb system [14]. Zeidler et al. studied the X-ray diffraction (XRD) for Ag–Ge–Se and the results are consistent with the presence of GeSe4 tetrahedra for all of the glass compositions and indicate a breakage of Se–Se homopolar bonds as silver is added to the Se-rich base glass [15]. Mohamed et al. studied the thermal stability of As–Se–Ag [16]. Kumar et al. reports the effect of Ag addition to Se–Sb glassy system [18]. They concluded that the silver doped alloys may be used for optoelectronic applications.

Due to the lack of long-range order (LRO), these glasses are characterized by the presence of various inherent defects and localized states in the gap. Studying electron

[a] e-mail: amshakra@yahoo.com

transport and gap states for amorphous semiconductors has a great interest due to their effect on the electrical properties [29,30].

This work aims to study the structural identification and the optical properties of $Se_{0.68}Ge_{0.24}Ag_{0.08}$ chalcogenide glass in thin film form. The value of the optical band gap E_g^{opt} and the type of optical transitions are deduced. Values of the refractive index n are analyzed to obtain the optical dispersion parameters E_o, E_d and the optical high frequency dielectric constant ε_∞. Finally the dependence of dielectric constant ε_1, dielectric loss ε_2, loss tangent tanδ, relaxation time τ and the optical conductivity σ_{opt} on photon energy $h\nu$ were carried out for $Se_{0.68}Ge_{0.24}Ag_{0.08}$ films.

2 Experimental procedures

Bulk glasses of $Se_{0.68}Ge_{0.24}Ag_{0.08}$ were synthesized using the melt-quenching method, from high purity (99.999%) Se, Ge and Ag elements. Components of the composition were weighed according to their atomic percentage and packed in evacuated (10^{-5} Torr) tubes of silica. These tubes were heated gradually in an oscillatory furnace up to 1273 K. They were held at this degree of temperature for 20 h. The molten material is then quenched in ice-cooled water to get amorphous sample. Thin films of the studied material were obtained from the bulk sample by the method of thermal evaporation on glass substrates under vacuum, using a coating unit (Edward E306A). The thickness of the thin film samples is measured by Tolansky's method [31].

Amorphicity of the studied samples in forms of powder and thin film were assured using XRD technique using X-ray diffractometer (PANalytical philips X'Pert PRODIFFRACTOMETER). Chemical composition of the studied samples was determined by energy dispersive X-ray analysis (EDX) using (JOEL 5400 scanning electron microscope. Spectral distribution of transmittance $T(\lambda)$ of $Se_{0.68}Ge_{0.24}Ag_{0.08}$ films at different thicknesses in the range (221.2–815.2 nm), was studied using unpolarized light at normal incidence by means of a double beam spectrophotometer (Type JASCO V-670) in the wavelength range (400–2500 nm) at room temperature (303 K). The experimental error in measuring the thickness of the film is ±2% and in $T(\lambda)$ is ±2%.

3 Results and discussion

3.1 Structural characterization

XRD was used to get information about the structure of $Se_{0.68}Ge_{0.24}Ag_{0.08}$, in thin film and powder forms. Figure 1 shows the XRD pattern of $Se_{0.68}Ge_{0.24}Ag_{0.08}$ in thin film and powder forms. The presence of only broad humps and without any sharp peaks is considered as an evidence for the amorphous structure of the investigated samples. The homogeneity of both bulk and thin film samples was checked by the determination of the elemental composition at random zones on the specimen surface, using the EDX analysis. The percentages of the constitutive elements are listed in Table 1. These percentages are found to be close to the prepared composition.

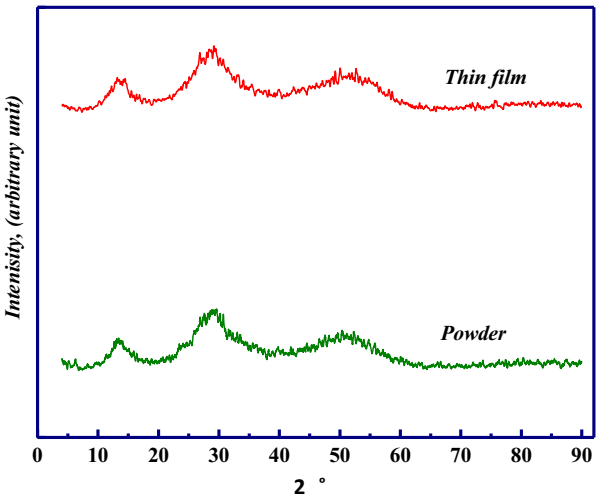

Fig. 1. X-ray diffraction (XRD) pattern of $Se_{0.68}Ge_{0.24}Ag_{0.08}$ in powder form and thin film form of thickness 543.3 nm as example.

Table 1. The EDX data of $Se_{0.68}Ge_{0.24}Ag_{0.08}$ films.

Composition	Se (at %)	Ge (at %)	Ag (at %)
$Se_{0.68}Ge_{0.24}Ag_{0.08}$	68.21	24.22	7.57

3.2 Optical properties of $Se_{0.68}Ge_{0.24}Ag_{0.08}$ thin film

3.2.1 The spectral distributions of $T(\lambda)$, (n), (k) and the absorption coefficient (α)

Figure 2 shows the spectral distribution curves of $T(\lambda)$ for $Se_{0.68}Ge_{0.24}Ag_{0.08}$ films of different thicknesses in the range (221.2–815.2 nm). Values of refractive index n and the absorption index k for $Se_{0.68}Ge_{0.24}Ag_{0.08}$ of different thicknesses were calculated from the measured $T(\lambda)$ using Swanepoel's method [32]. The error in the method used to calculate the values n and k is about ±1.0%. The values obtained for n and k are thickness independent. The spectral distribution of the average values of n and k for all thicknesses is shown in Figures 3 and 4, respectively. The decrease of n with increasing wave length (λ) indicates the normal dispersion behavior and it is also considered an indicator of the presence of several interactions between the electrons and the incident photons in the studied composition. From the obtained values of k we can calculate the absorption coefficient α from the relation $\alpha = 4\pi k/\lambda$. Figure 5 illustrates the plot of logα versus photon energy $h\nu$ for $Se_{0.68}Ge_{0.24}Ag_{0.08}$ films. The curve in this figure could be divided into two regions [33,34]:

(i) Region one: for values of $\alpha \geq 10^4$ cm^{-1}. This is in line with the transitions between extended states in both conduction and valence bands, where the law of Tauc is valid [33,34]:

$$\alpha h\nu = A\,(h\nu - E_g^{opt})^r, \quad (1)$$

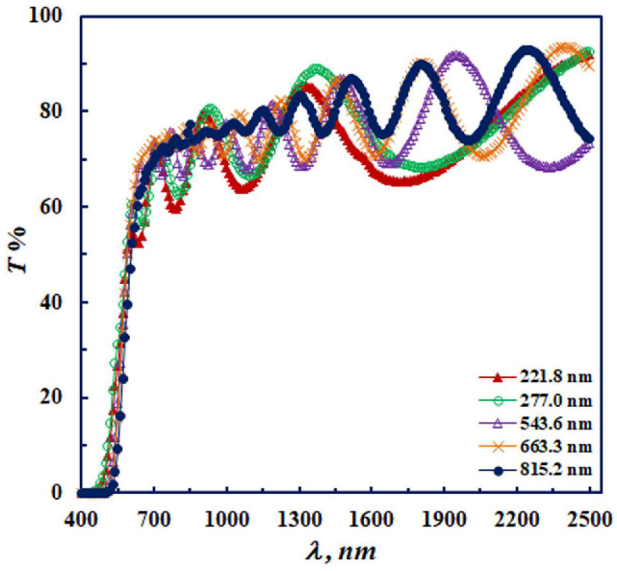

Fig. 2. Spectral distribution of transmission $T(\lambda)$ for $Se_{0.68}Ge_{0.24}Ag_{0.08}$ of different thicknesses.

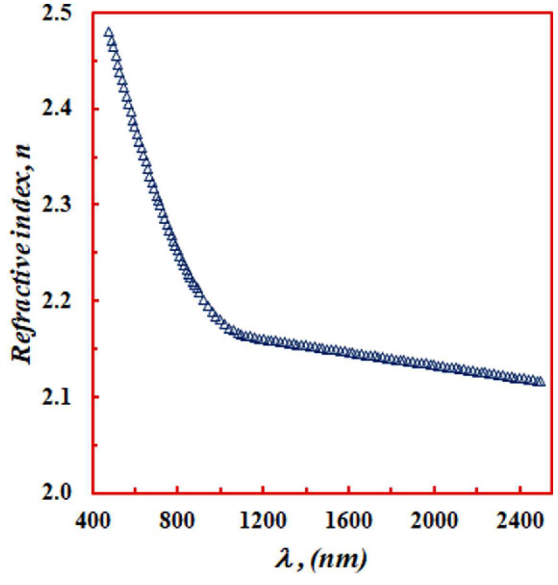

Fig. 3. The dependence of the average values of refractive index n on λ for $Se_{0.68}Ge_{0.24}Ag_{0.08}$ films.

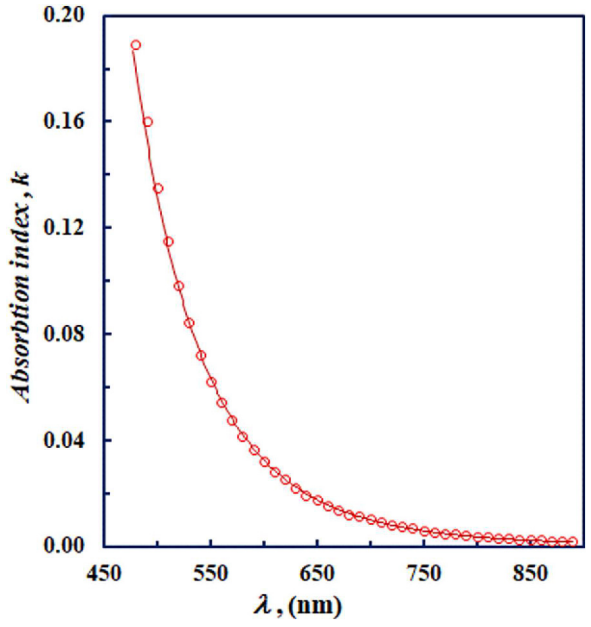

Fig. 4. The dependence of the average values of the absorption index k on λ for $Se_{0.68}Ge_{0.24}Ag_{0.08}$ films.

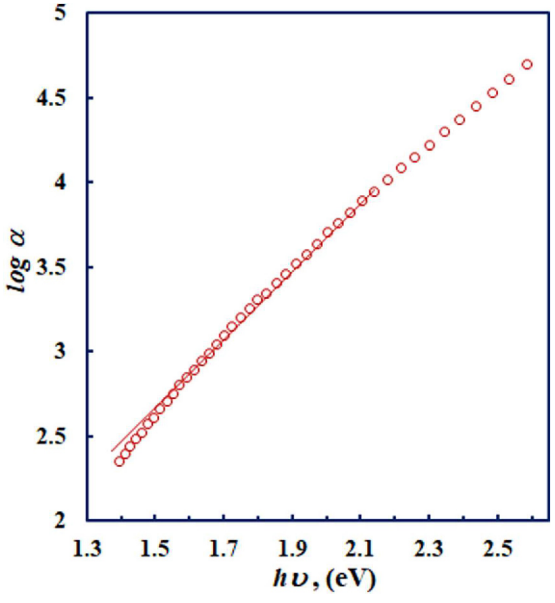

Fig. 5. Plots of logα as a function of photon energy $h\nu$ for $Se_{0.68}Ge_{0.24}Ag_{0.08}$ films.

where A is a constant expressing the quality of the film, r is a number representing the type of the transition and $E_{g(1)}^{\text{opt}}$ is the optical energy gap. The parameter r has the value 2 for indirect transition and 0.5 for direct transition. In order to determine the value of $E_{g(1)}^{\text{opt}}$, a graph of $(\alpha h\nu)^{1/r}$ versus $h\nu$ is plotted. The relations $(\alpha h\nu)^{1/2}$ and $(\alpha h\nu)^{2}$ versus $h\nu$ are plotted in Figure 6 for $Se_{0.68}Ge_{0.24}Ag_{0.08}$ films. This figure shows that, the relation $(\alpha h\nu)^{\frac{1}{2}} = f(h\nu)$ is linear, which indicates that the allowed transitions are indirect. Extrapolating the linear part of the relation $(\alpha h\nu)^{\frac{1}{2}} = f(h\nu)$ to the $h\nu$ axis gives $E_{g(1)}^{\text{opt}}$ and the value of constant A can be calculated from the slope of this linear part. The obtained values of $E_{g(1)}^{\text{opt}}$ and A are given in Table 2, and it is found to be in good agreement with that obtained before by Abd-Elrahman et al. [13].

The value of $E_{g(2)}^{\text{opt}}$ could be obtained also by the relation between $h\nu\sqrt{\varepsilon_2}$ versus $h\nu$ near the absorption edge (where $\varepsilon_2 = 2nk$ is the imaginary part of dielectric constant), as shown in Figure 7. The linear part of the curve can follow the equation [34]:

$$h\nu\sqrt{\varepsilon_2} \approx (h\nu - E_{g(2)}^{\text{opt}}). \quad (2)$$

Table 2. Optical constants and the parameters E_o, E_d of $Se_{0.68}Ge_{0.24}Ag_{0.08}$ films.

$E^{opt}_{g(1)}$ eV From equation (1)	A, $cm^{-1}eV^{-1}$	E_e, eV	$E^{opt}_{g(2)}$, eV From equation (2)	E_o, eV	E_d, eV
1.90 ± 0.02	2.54×10^5	0.50 ± 0.01	1.91 ± 0.02	5.36 ± 0.05	18.86 ± 0.05

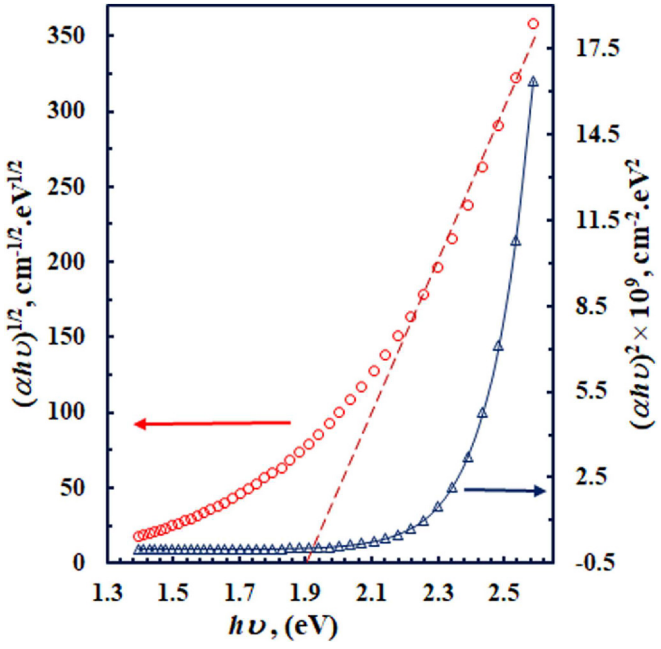

Fig. 6. Dependence of $(\alpha h\nu)^{1/2}$ and $(\alpha h\nu)^2$ on the photon energy $h\nu$ for $Se_{0.68}Ge_{0.24}Ag_{0.08}$ films.

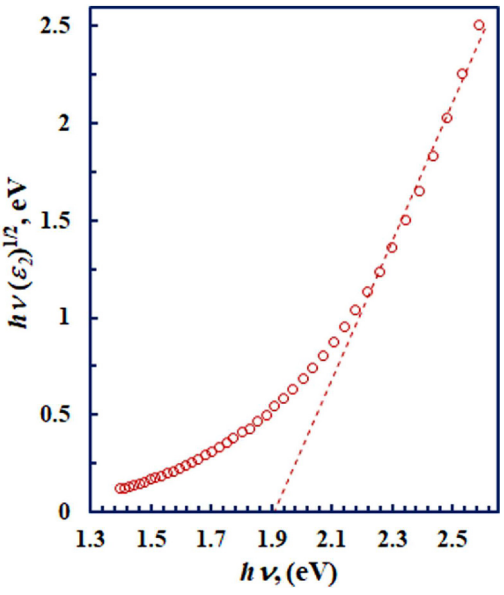

Fig. 7. Dependence of $h\nu(\varepsilon_2)^{1/2}$ on the photon energy $h\nu$ for $Se_{0.68}Ge_{0.24}Ag_{0.08}$ films.

The obtained linear line represents the indirect optical transitions [34]. Extrapolation of the linear part gives $E^{opt}_{g(2)}$ for the investigated composition (given also in Tab. 2). The value of $E^{opt}_{g(2)}$ calculated from Figure 7 corresponds well with the value of $E^{opt}_{g(1)}$ calculated above from Figure 6.

(ii)Region two: for values of, $\alpha < 10^4$ cm^{-1}, the absorption usually obeys the Urbach rule [35] i.e.,

$$\alpha(v) = \alpha_0 \exp(h\nu/E_e), \tag{3}$$

where α_0 is a constant and E_e is the energy Urbach tail, which represents the degree of disorder in non-crystalline materials [36]. The value of E_e is estimated from the slope of the linear part of the relation between logα and $h\nu$, as shown in Figure 5, and given in Table 2. In this region, the absorption is due to transitions between localized states in the exponential tail in one band and extended states of the other band [37].

3.2.2 Dispersion energy parameters E_o and E_d

To determine the single-oscillator E_o and dispersion energy E_d (dispersion energy parameters), we can use a single oscillator characterization for frequency-dependent dielectric constant as proposed by Wemple and DiDomenico [38,39]. The relation between n and the single oscillator constants (E_o and E_d) is given by [39,40]:

$$(n^2-1)^{-1} = \frac{[E_o^2 - (h\nu)^2]}{E_o\, E_d}. \tag{4}$$

Figure 8 shows the plot of $(n^2-1)^{-1}$ versus $(h\nu)^2$ for the examined composition films. It represents a straight line, its slope of $(E_0E_d)^{-1}$ and an intercept with y-axis of (E_0/E_d). The calculated values of E_o and E_d are listed in Table 2. The obtained curve indicates a deviation from linearity to positive curvature at the short and long wavelengths. This deviation from linearity at the shorter wavelengths may be attributed to the excitonic absorption and at the longer wavelengths may be due to the negative contribution of the lattice vibrations on index of refraction n [38,39]. Based on the single-oscillator model, the parameters E_o and E_d are related to the imaginary part of dielectric constant $\varepsilon_2(\omega)$ and the moments M_{-1} and M_{-3} of the $\varepsilon_2(E)$ optical spectrum by [39,40]:

$$E_0^2 = \frac{M_{-1}}{M_{-3}} \quad \& \quad E_d^2 = \frac{M_{-1}^3}{M_{-3}}. \tag{5}$$

The rth moment M_r of the $\varepsilon_2(E)$ spectrum is given by:

$$M_r = \frac{2}{\pi}\int_{E_r}^{\infty} E^r \varepsilon_2(E)\, dE, \tag{6}$$

where $E = h\nu$ and E_t is the absorption threshold energy. Refractive n and absorption k indices are related

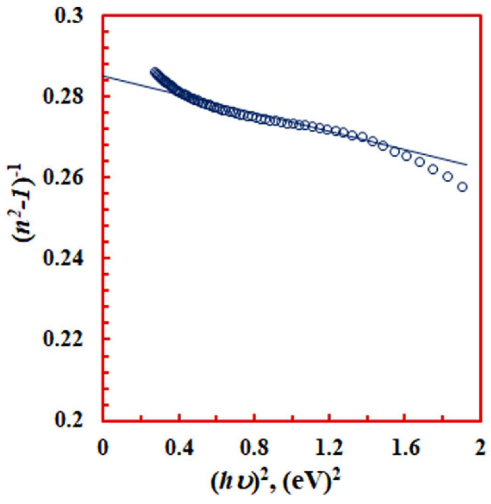

Fig. 8. A plot of $(n^2 - 1)^{-1}$ against $(h\nu)^2$ for $Se_{0.68}Ge_{0.24}Ag_{0.08}$ films.

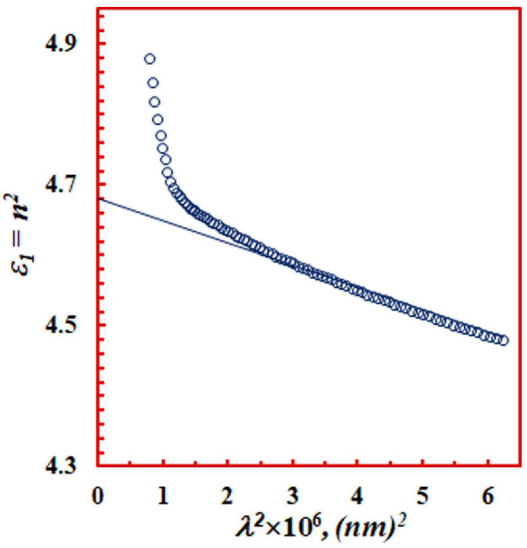

Fig. 9. A plot of ε_1 as a function of λ^2 for $Se_{0.68}Ge_{0.24}Ag_{0.08}$ films.

to the imaginary part of complex dielectric constant $\varepsilon(\omega) = \varepsilon_1(\omega) + i\,\varepsilon_2(\omega)$, where $\varepsilon_1(\omega)$ is the real part of dielectric constant and ω is the frequency of photon. All information about the electronic excitation spectrum of the material is contained in $\varepsilon_1(\omega)$ or $\varepsilon_2(\omega)$, since $\varepsilon_1(\omega)$ is related to $\varepsilon_2(\omega)$ by the relation of Kramers–Kroning [39].

Equation (5) shows that, E_o is independent of the scale of $\varepsilon_2(\omega)$ (the numerator and denominators are of the same power) and is consequently an average energy gap, whereas E_d depends on the scale of $\varepsilon_2(\omega)$, and therefore serves as an interband strength parameter. Since the moments M_{-1} and M_{-3} are included in the calculation of E_o and E_d values, the $\varepsilon_2(\omega)$ spectrum is highly weighted near the interband absorption threshold. In addition, the oscillator energy E_o is corresponds to the energy difference between the centers of gravity of the V.B. and C.B. [40]. This value differs from the optical gap E_g^{opt} that detects the optical properties near the band edges of the material. Thus, E_o is associated with the average molar bond energy of the various bonds in the material. By using the obtained values of E_o and E_d we can calculate M_{-1} and M_{-3} from equation (5) for $Se_{0.68}Ge_{0.24}Ag_{0.08}$ films and found to equal 3.52 and 0.123 eV^{-2}, respectively.

3.2.3 Determination of the high frequency dielectric constant ε_∞

In the transparent region ($k = 0$), the values of n can be used to get the value of ε_∞ by two methods [41]. The first one distinguishes the lattice vibrational modes and the free carriers contribution. The second method is depending on the dispersion resulting from the carriers bound in an empty lattice. These two methods are used to calculate the value of ε_∞ ($\varepsilon_{\infty(1)}$ and $\varepsilon_{\infty(2)}$) as follows:

(i) The first method

The real part of dielectric constant ε_1 ($\varepsilon_1 = n^2$) is given by [41]:

$$\varepsilon_1 = \varepsilon_{\infty(1)} - \left(\frac{e^2 N}{4\pi^2\, c^2 \varepsilon_0 m^*}\right) \lambda^2, \tag{7}$$

where N is the concentration of free charge-carriers, e the charge of electron, m^* the effective mass of the electron, ε_o the free space permittivity and c the velocity of light. By plotting the relation between ε_1 and λ^2 for $Se_{0.68}Ge_{0.24}Ag_{0.08}$ as shown in Figure 9, we can calculate (N/m^*) and $\varepsilon_{\infty(1)}$ from the slope and intersection of the linear part of this curve. These values are given in Table 3.

(ii) The second method

The dispersion of n can be also analyzed to calculate ε_∞ by the model of single oscillator [38,39]. The linear relation between $(n^2 - 1)^{-1}$ and λ^{-2} shown in Figure 10 suggested that n of the investigated composition follows Sellmeier's dispersion equation [41]:

$$(n^2 - 1)^{-1} = \frac{[1 - (\lambda_o/\lambda)^2]}{(n_\infty^2 - 1)^2}, \tag{8}$$

$$\left(n_\infty^2 - 1\right) = S_o\, \lambda_o^2, \tag{9}$$

where n_∞ is the refractive index at infinite wavelength, λ_0 and S_o are the average oscillator wavelength and strength, respectively. Values of n_∞^2 ($\varepsilon_{\infty(2)}$) and λ_0 can be calculated from extrapolating of the obtained line to the y-axis and the slope of the linear part of Figure 10, respectively. The obtained values of $\varepsilon_{\infty(2)}$, λ_0 and S_o (calculated from Eq. (9)) are listed in Table 3. The values of $\varepsilon_{\infty(1)}$ and $\varepsilon_{\infty(2)}$ obtained by the two methods are in agreement with each other. Although there is a difference in the two methods used to calculate ε_∞, this agreement is due to the fact that the lattice-vibrations and the frequencies of plasma ω_p are separated from the frequency of the absorption band-edge.

According to the theory of Penn's [42]:

$$n^2 = 1 + (h\,\omega_p/E_g^{\text{opt}})^2, \tag{10}$$

Table 3. The parameters $\varepsilon_{\infty(1)}$, $\varepsilon_{\infty(2)}$, N/m^*, S_o, λ_0 and ω_p for $Se_{0.68}Ge_{0.24}Ag_{0.08}$ films.

$\varepsilon_{\infty(1)}$ From equation (6)	N/m^*, m^{-3}	$\varepsilon_{\infty(2)}$ From equation (8)	S_o, m^{-2}	λ_0, nm	ω_p, m^{-1}
4.68 ± 0.04	3.87×10^{55}	4.52 ± 0.04	7.14×10^{13}	222.0 ± 0.8	1.56×10^{14}

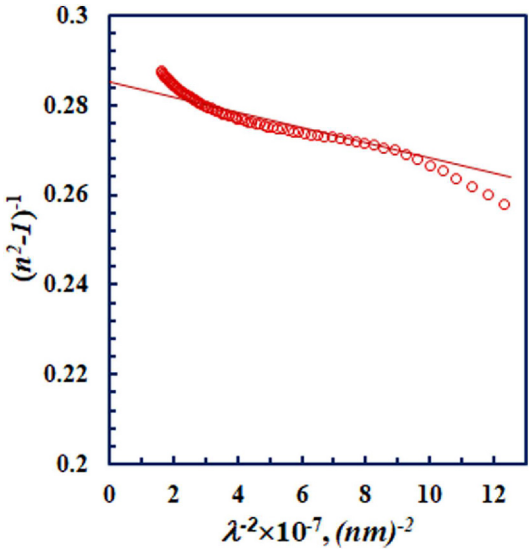

Fig. 10. A plot of $(n^2-1)^{-1}$ as a function of λ^{-2} for $Se_{0.68}Ge_{0.24}Ag_{0.08}$ amorphous films.

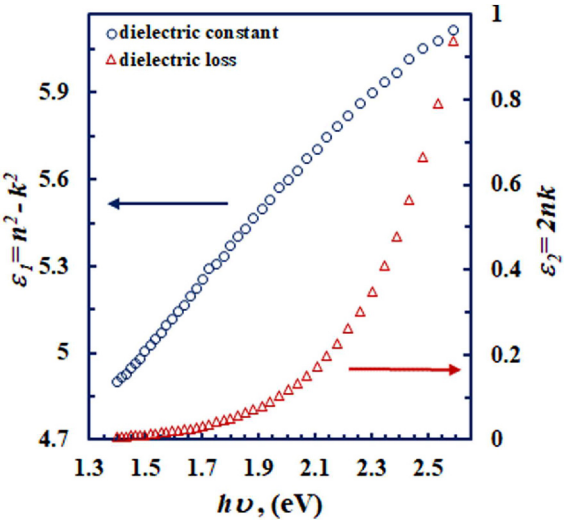

Fig. 11. Plots of ε_1 and ε_2 as a function of $h\nu$ for $Se_{0.68}Ge_{0.24}Ag_{0.08}$ films.

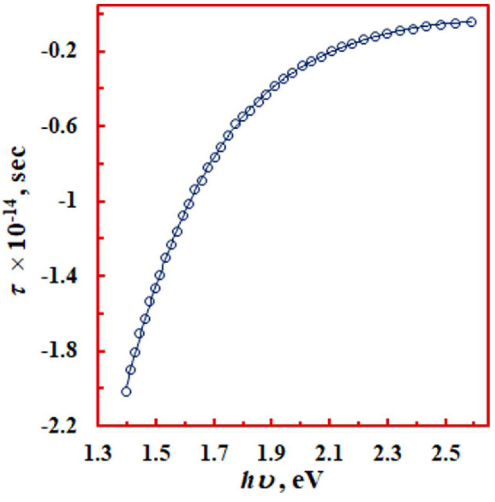

Fig. 12. Dependence of the dielectric relaxation time τ on the photon energy $h\nu$ for $Se_{0.68}Ge_{0.24}Ag_{0.08}$ films.

where ω_p is the frequency of plasma, which is defined as the resonance frequency of the free oscillations of electrons around their equilibrium positions, and given by:

$$\omega_p^2 = \frac{e^2\, N}{\varepsilon_0 \varepsilon_\infty\, m^*}. \tag{11}$$

Using the value of N/m^* given in Table 3, ω_p is calculated from equation (11) and is given also in the same table.

3.2.4 The complex dielectric constant near the absorption edge

The real ε_1 part and imaginary (dielectric loss) ε_2 parts of dielectric constant were determined from the following equations [41,43]:

$$\varepsilon_1 = n^2 - k^2, \tag{12}$$

and

$$\varepsilon_2 = 2nk = \left(\frac{\varepsilon_\infty\, \omega_p^2}{8\,\pi^2\, c^3\, \tau}\right) \lambda^3, \tag{13}$$

where τ is the dielectric relaxation time. The values of ε_1 and ε_2 can be calculated for the studied composition as they are related to the density of states in the forbidden energy gap [43]. Variation of ε_1 and ε_2 with $h\nu$ is shown in Figure 11 for $Se_{0.68}Ge_{0.24}Ag_{0.08}$ films. It is clear that both ε_1 and ε_2 increase with $h\nu$. The property that is closely related to the conductivity of a solid is a dielectric relaxation time τ, it can be calculated by the equation [44,45]:

$$\tau = \frac{\varepsilon_\infty - \varepsilon_1}{\omega\, \varepsilon_2}, \tag{14}$$

where ω is the angular frequency. Figure 12 represents the variation of τ versus $h\nu$ for $Se_{0.68}Ge_{0.24}Ag_{0.08}$ thin films. This figure shows that, τ is enhanced with increasing $h\nu$.

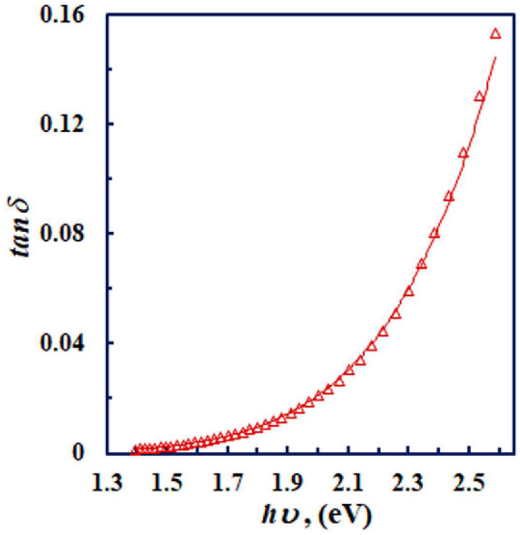

Fig. 13. Dependence of the dissipation factor tanδ on the photon energy $h\nu$ for $Se_{0.68}Ge_{0.24}Ag_{0.08}$ films.

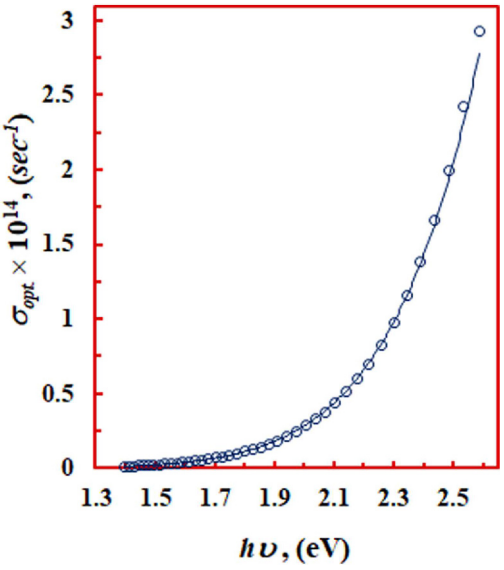

Fig. 14. Dependence of optical conductivity σ_{opt} on the photon energy $h\nu$ for $Se_{0.68}Ge_{0.24}Ag_{0.08}$ films.

3.2.5 Calculating the loss tangent (tanδ) and optical conductivity (σ_{opt})

The factor of dissipation (loss tangent) tanδ can be evaluated by [46]:

$$\tan\delta = \frac{\varepsilon_2}{\varepsilon_1}. \tag{15}$$

The variation of tanδ with $h\nu$ for the investigated composition is shown in Figure 13. It is obvious from this figure that, tanδ increases with frequency.

Optical conductivity σ_{opt} can be calculated from the absorption coefficient α as follows [47]:

$$\sigma_{\text{opt}} = \frac{n\, c\, \alpha}{4\pi}. \tag{16}$$

Figure 14 illustrates the variation of optical conductivity σ_{opt} with $h\nu$. It is clear that, σ_{opt} increases with $h\nu$. At high photon energies, the increase of σ_{opt} can be explained by the high absorption of $Se_{0.68}Ge_{0.24}Ag_{0.08}$ films and also, the excitation of electrons by increasing the energy of photon $h\nu$ [48].

From all the above obtained results in the present study and previously obtained for Se–Ge [45], we can see that, by adding Ag to Se–Ge the values of E_g^{opt} decrease, while E_e and ε_∞ increase. This can be interpreted as follows: the structure of Ge–Se (binary glass) has a short-range order (SRO) tetrahedral where the atom of Ge surrounded by 4 selenium atoms [49,50]. Adding Ag atoms to Se–Ge interacts primarily with Se and breaks the covalent network to leave Ge–$Se_{4/2}$ tetrahedral structure [51]. It is also assumed that Ag atoms act to disassemble the Ge–Se structure during the formation of Ag–Se ion bonds [52], so the observed decrease in E_g^{opt} with Ag addition is explained by the decrease in bond energy between Se and Ag, where the bond energy for Se–Ge and Se–Ag are 5.08 and 3.53 eV, respectively [53,54]. Moreover, the values of the dielectric constant are directly related to the density of states within the forbidden gap [43]. So, the obtained increase of dielectric constant by adding Ag to Se–Ge can be explained by the corresponding increase of the value of the width of the tail of localized states E_e in the band-gap (from 0.4537 to 0.496 eV) and the value of N/m^* (from 3.68×10^{54} to 3.87×10^{55} m^{-3}) and therefore decrease in optical band gap E_g^{opt} (from 2.02 to 1.9 eV).

4 Conclusion

Amorphous films of $Se_{0.68}Ge_{0.24}Ag_{0.08}$ were prepared by thermal evaporation method with different thicknesses in the range (221.2–815.2 nm). XRD pattern confirms the amorphicity of the investigated films. The optical constants n and k were calculated from the spectral distribution of $T(\lambda)$ for the studied composition of different thicknesses using Swanepoel's method. The method proposed by Swanepoel's was applied to the studied films and is valid with high accuracy for calculating the optical constants of $Se_{0.68}Ge_{0.24}Ag_{0.08}$ thin films. The obtained values of n and k are found to be thickness independent. The analysis of the absorption coefficient α according to Tauc's model gives the optical energy gap $E_{g(1)}^{\text{opt}}$=1.902 eV. The obtained results showed that the allowed transitions in the investigated samples are indirect. Dispersion parameters E_o, E_d and the high frequency and $\varepsilon_{\infty(1)}$ were also obtained and found to be 5.356 eV, 18.86 eV and 4.68, respectively.

References

1. C. Tsay, Y. Zha, C. Arnold, Opt. Express **18**, 26744 (2010)
2. Yu. Mourzina, M.J. Schoning, J. Schubert, W. Zander, A.V. Legin, Yu.G. Vlasov, P. Kordos, H. Luth, Sens. Actuators B: Chem. **71**, 13 (2000)

3. V. Ta'eed, N. Baker, L. Fu, K. Finsterbusch, M. Lamont, D. Moss, H.H. Nguyen, B. Eggleton, D. Choi, S. Madden, B. Luther-Davies, Opt. Express **15**, 9205 (2007)
4. A. Redaelli, A. Pirovano, F. Pellizzer, A.L. Lacaita, D. Ielmini, R. Bez, IEEE Electron Device Lett. **25**, 684 (2004)
5. T.K. Todorov, K.B. Reuter, D.B. Mitzi, Adv. Mater. **22**, E156 (2010)
6. A.V. Kolobov, J. Tominaga, *Chalcogenides: Metastability and Phase Change Phenomena* (Springer, Berlin, 2010)
7. N.A. Hegab, A.S. Farid, A.M. Shakra, M.A. Afifi, A.M. Alrebati, J. Electro. Mater. **45**, 3332 (2016)
8. A.K. Kukreti, S. Gupta, M. Saxena, N. Rastogi, Int. J. Innovative Res. Sci. Eng. Technol. **4**, 18608 (2015)
9. B.A. Mansour, S.A. Gada, H.M. Eissa, J. Non-Cryst. Solids **412**, 53 (2015)
10. H.E. Atyia, N.A. Hegab, Physica B **454**, 189 (2014)
11. M. Mohamed, Mater. Res. Bull. **65**, 243 (2015)
12. D. Singh, S. Kumar, R. Thangara, J. Phase Transitions **87**, 19 (2014)
13. M.I. Abd-Elrahman, A.Y. Abdel-Latief, R.M. Khafagy, N. Younis, M.M. Hafiz, Mater. Sci. Semicond. Process. **24**, 21 (2014)
14. A. Dahshana, H.H. Hegazy, K.A. Aly, P. Sharma, Physica B **526**, 117 (2017)
15. A. Zeidler, P.S. Salmon, D.A.J. Whittaker, A. Piarristeguy, A. Pradel, H.E. Fischer, C.J. Benmore, O. Gulbiten, R. Soc. Open Sci. **5**, 171401 (2018)
16. M. Mohamed, M.N. Abd-el Salam, M.A. Abdel-Rahim, A.Y. Abdel-Latief, E.R. Shaaban, J. Therm. Anal. Calorim., **132**, 91 (2018)
17. S. Tiwari, A.K. Saxena, Adv. Appl. Sci. Res. **2**, 382 (2011)
18. A. Kumar, S.K. Tripathi, A. Kumar, Acta Phys. Pol. A. **129**, 1178 (2016)
19. K.A. Aly, A. Dahshan, I.S. Yahia, Philos. Mag. **92**, 912 (2012)
20. S. Mahadevan, A. Giridhar, J. Non-Cryst. Solids **197**, 219 (1996)
21. A. Zakery, S.R. Elliott, J. Non-Cryst. Solids **330**, 1 (2003)
22. F. Jiang, M. Jiang, L. Hou, F. Gan, M. Okuda, Jpn. J. Appl. Phys. Suppl. **28**, 293 (1989)
23. T. Kawaguchi, S. Maruno, J. Appl. Phys. **77**, 628 (1995)
24. A. Kolobov, S. Elliott, Adv. Phys. **40**, 625 (1991)
25. Y.Y. Chang, L.H. Chou, Jpn. J. Appl. Phys. Part 2, **39**, L294 (2000)
26. T. Wagner, M. Frumar, S.O. Kasap, Mir. Vlcek, Mil. Vlcek, J. Optoelectron. Adv. Mater. **2**, 227 (2001)
27. Z.U. Borisova, *Glassy Semiconductors* (Plenum Press, New York, 1981)
28. M. Ohto, M. Itho, K. Tanaka, J. Appl. Phys. **77**, 1034 (1995)
29. W. Beyer, H. Mell, J. Stuke, Phys. Status Solidi B **45**, 153 (1971)
30. V.I. Mikla, V.V. Mikla, *Metastable States in Amorphous Chalcogenide Semiconductors* (Springer, Berlin, 2010)
31. S. Tolansky, *Multiple-beam Interference Microscopy of Metals*, (Academic Press, London, 1970)
32. R. Swanepoel, J. Phys. E: Sci. Instrum. **16**, 1214 (1983)
33. J. Tauc, *Amorphous and Liquid Semiconductors* (Plenum Press, London and New York, 1974)
34. J. Tauc, R. Grigorovici, A. Vancu, Phys. Status Solidi B **15**, 627 (1966)
35. F. Urbach, Phys. Rev. **92**, 1324 (1953)
36. J. Olley, Solid State Commun. **13**, 1437 (1973)
37. M. Suzuki, H. Ohdaira, T. Matsumi, M. Kumeda, T. Shimizu, Jpn. J. Appl. Phys. **16**, 221 (1977)
38. M. DiDomenico, S.H. Wemple, J. Appl. Phys. **40**, 720 (1969)
39. S.H. Wemple, M. DiDomenico, Phys. Rev. B **3**, 1338 (1971)
40. S.H. wimple, M. DiDomenico, Phys. Rev. Lett. **23**, 1156 (1969)
41. J.N. Zemel, J.D. Jensen, R.B. Schoolar, Phys. Rev. **140**, A330 (1965)
42. D.D. Minkov, E. Vateva, E. Skordeva, D. Arsova, M. Nikiforova, G. Nadjakov, J. Non-Cryst. Solids **90**, 481 (1987)
43. A. El-Korashy, H. El-Zahed, M. Radwan, Physica B **334**, 75 (2003)
44. M.M. Abdel-Aziz, I.S. Yahia, L. A. Wahab, M. Fadel, M.A. Afifi, Appl. Surf. Sci. **252**, 8163 (2006)
45. E.G. El-Metwally, M.O. Abou-Helal, I.S. Yahia, J. Ovonic Res. **4**, 20 (2008)
46. F. Yakuphanoglu, A. Cukurovali, I. Yilmaz, Physica B **351**, 53 (2004)
47. J.I. Pankove, *Optical Processes in Semiconductors* (Dover Publications Inc., New York, 1975)
48. F. Yakuphanoglu, A. Cukurovali, I. Yilmaz, Opt. Mater. **27**, 1363 (2005)
49. R. Azoulay, H. Thibierge, A. Brenac, J. Non-Cryst. Solids **18**, 33 (1975)
50. N. Ramesh Rao, P.S.R. Krishna, S. Basu, B.A. Dasannacnarya, K.S. Sangunni, E.S.R. Gopal, J. Non-Cryst. Solids **240**, 221 (1998)
51. R. Dejus, S. Susman, K. Volin, D. Montague, D. Price, J. Non-Cryst. Solids **143**, 162 (1992)
52. T. Kawaguchi, S. Maruno, S.R. Elliot, J. Appl. Phys. **79**, 12 (1996)
53. J.A Dean, *Lange's Hand Book of Chemistry*, 14th edn. (University of Tennessee, Knoxville, 1992)
54. S.S. Fouad, A.E. Bekheet, A.M. Farid, Physica B **322**, 163 (2002)